Chapter 21
A Synchrotron Photoluminescence Microscopy Study into the Use and Degradation of Zinc White in 'The Woodcutters' by Bart van der Leck

Selwin Hageraats, Katrien Keune, Mathieu Thoury, and Ruth Hoppe

21.1 Introduction

Bart van der Leck, who—together with Piet Mondrian and Theo van Doesburg—co-founded the artistic movement *De Stijl,* stood at the forefront of early abstract art. Van der Leck's works are constructed from a profound, well-documented vision on color, space, geometry and light, resulting in a style in which composition is key, and arrangements are often subject to revision. Between 1916 and 1918, Van der Leck's works became increasingly more abstract. He made series of so-called *compositions*, in which the starting point is often a sketch or study with a figurative depiction of his subject. In subsequent steps he then reduces the composition into an increasingly

S. Hageraats (✉)
Department of Conservation and Science, Rijksmuseum, Amsterdam, The Netherlands

IPANEMA, CNRS, Ministère de la Culture, UVSQ, USR3461, Université Paris-Saclay, Gif-sur-Yvette, France

Van 't Hoff Institute for Molecular Sciences, University of Amsterdam, Amsterdam, The Netherlands
e-mail: s.hageraats@rijksmuseum.nl

K. Keune
Department of Conservation and Science, Rijksmuseum, Amsterdam, The Netherlands

Van 't Hoff Institute for Molecular Sciences, University of Amsterdam, Amsterdam, The Netherlands
e-mail: k.keune@rijksmuseum.nl

M. Thoury
IPANEMA, CNRS, Ministère de la Culture, UVSQ, USR3461, Université Paris-Saclay, Gif-sur-Yvette, France
e-mail: mathieu.thoury@synchrotron-soleil.fr

R. Hoppe
Gemeentemuseum Den Haag, Den Haag, The Netherlands
e-mail: rhoppe@gemeentemuseum.nl

K. J. van den Berg et al. (eds.), *Conservation of Modern Oil Paintings*,
https://doi.org/10.1007/978-3-030-19254-9_21

more abstract representation of the subject, in which the forms are transformed into rectangles or other geometric shapes floating on a white background, constituting the essence of the subject. In these abstract compositions he would only work with primary colors, black, and grey [1, 2]. *The Woodcutters*, (oil on canvas, 157 × 182.5 cm, Fig. 21.1a), painted in 1928 and depicting two woodcutters cutting down a tree, is representative for his work from 1919 onwards; when Van der Leck broke with the *De Stijl* movement. It was in this period that he moved away from highly abstracted forms to compositions in which the subject is yet again more readable.

In a recently published report of a technical study of *The Woodcutters,* it is described that under ultraviolet (UV) light the white background exhibits green luminescence in three distinctly different intensities [3]. As can be seen in Fig. 21.1b, the lowest intensity is predominantly visible in the lower left part of the painting, while an intermediate intensity can be observed in the top half, and the brightest luminescence dominates in the lower half of the painting. Although most of the differently luminescing paint areas were impossible to differentiate without the use of UV-light, in some areas of the background, such as those directly surrounding the color planes, differences in luminescence could be observed to correspond to slight variations in color and surface texture. It was found that the sole pigment used in the top layer of this white background is zinc white, which is most likely mixed with linseed oil as a binding medium. Although it must be noted that both zinc white and linseed oil are known to exhibit green luminescence [4, 5], in this report, the differences in appearance of the background under UV were ascribed to the use of different types of zinc white. Considering the known variation in luminescence behavior among different batches of zinc white [6], and the established use of UV photography for the identification of zinc white in oil paintings [7, 8], it is indeed presumed likely that the appearance of the background under UV is primarily related to the use of zinc white.

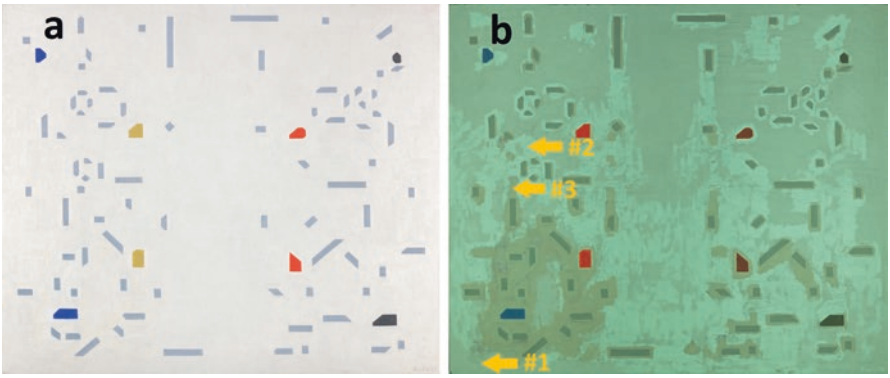

Fig. 21.1 Bart van der Leck's *The Woodcutters* (**a**) photographed under white light (© Bart van der Leck c/o Pictoright Amsterdam 2019) (**b**) photographed under UV light (© Gemeentemuseum Den Haag). Yellow arrows indicate the three sampling locations: sampling location #1 exhibits an intermediate intensity, sampling location #2 a bright intensity, and sampling location #3 a low intensity of green luminescence

The luminescence behavior of zinc white (ZnO) originates from its semiconductor properties. ZnO is a (direct) wide band gap II-IV semiconductor with a band gap of 3.3 eV (~375 nm) at room temperature [9]. Defects in the ZnO crystal structure, such as vacancies and interstitials, introduce energy levels within the band gap. These energy levels are often called trap states, and result in additional radiative relaxation pathways [9, 10]. Although the green trap state emission (~500–550 nm) is the most prominent and most often observed, emissions in the blue and red are also reported. Differences in the relative intensities of these trap state emissions and the band gap emission have been reported for different batches of zinc white, and allow discrimination between zinc whites based on their photoluminescence behavior [6].

In order to examine whether different types of zinc white are indeed present in the white background, it was proposed to study microscopic cross-sections using the same novel photoluminescence micro-imaging method as used by Bertrand et al. [6], and employ a newly developed computational method to detect statistical differences between zinc whites in different paint layers. The aforementioned photoluminescence micro-imaging technique makes use of synchrotron-generated deep-UV excitation and a multispectral acquisition approach [11, 12]. Besides its ability to resolve submicrometric particles and examine their luminescence behavior, its deep-UV excitation capabilities allow access to an emission range with energies exceeding the ZnO band gap. It has been shown in a previous study [13] that in this range, zinc white exhibits no emission and more weakly luminescing compounds, such as zinc white degradation products, can be detected. As the (surface) degradation of zinc white may also have an effect on the macroscale luminescence, using the novel photoluminescence micro-imaging technique, two aspects that influence this phenomenon can be examined simultaneously. Yet, since photoluminescence micro-imaging does not provide a chemically specific probe for all pigments and degradation products, complementary methods of analysis need to be employed in parallel. In this study, optical microscopy and SEM-EDX were used to complement the photoluminescence data in helping to resolve the painting build-up and identifying degradative surface layers.

21.2 Experimental

21.2.1 Sample Preparation

All analyses were performed on three samples taken from the locations indicated in Fig. 21.1b. The regions from which the paint samples were taken were chosen so as to represent each of the three different intensity levels of green luminescence. Paint samples were embedded in Technovit® 2000 LC resin, and dry polished with silicon carbide polishing cloths (Micro-Mesh®, final step 12.000 mesh) to be prepared as cross-sections.

21.2.2 Instrumental Analysis

Optical Microscopy Cross-sections were analyzed using a Zeiss Axio Imager. A2m optical microscope. The microscope was equipped with visible and UV LEDs, to provide white and UV light respectively. Images under UV light were recorded by filtering the excitation beam with a Zeiss G 365 band-pass filter and diverting the lower energy emission using a beam splitter with a cut-off wavelength of 395 nm. Emission was subsequently filtered with a 420 nm low-pass filter and recorded using a AxioCam MRc5 camera.

SEM-EDX Scanning electron microscopy images were recorded using a Thermo Fisher Nova Nano SEM 450 electron microscope. Backscattered electron images were taken at a 15 kV accelerating voltage and eucentric working distances between 5 and 6 mm. For the purpose of pigment identification, EDX analysis was performed using the coupled Thermo Fisher EDX system. Cross-sections were gold coated (3 nm thickness) in a Quorum Technologies SC7640 gold sputter coater prior to SEM-EDX analysis in order to improve surface conductivity.

S-DUV-PL Micro-Imaging Synchrotron deep-UV multispectral photoluminescence micro-imaging was performed at the DISCO beamline of the SOLEIL synchrotron. The optical set-up has been described in detail in Thoury et al. [12], so the focus here will be on the used parameters and the choice of exchangeable optics. All three cross-sections were analyzed with an excitation energy of 4.43 eV (280 nm), and a dichroic mirror with a cut-off wavelength of 300 nm. Four emission filters were used to record photoluminescence images: 327–353, 370–410, 412–438, and 499–529 nm. The three longer wavelength filters are meant to specifically transmit ZnO band gap emission, blue ZnO trap state emission, and green ZnO trap state emission respectively. It is worth noting that it is exactly this green ZnO trap state emission that gives the painting its green luminescence on the macroscale. Variable exposure times were used so as to ensure the highest possible signal, without reaching saturation. For the 327–353 nm emission filter, exposure times were set between 70 and 370 seconds, whereas for the remaining filters, due to the bright ZnO emission, exposure times could be set between 2.5 and 22 s. A Zeiss Ultrafluar 100 × UV-transmitting immersion objective was used, capable of resolving the individual submicrometric zinc white particles.

21.2.3 Image Processing & Statistical Analysis

Due to the limited field of view of the 100 × objective used in the S-DUV-PL micro-imaging set-up, composite images were recorded in a mosaic-like manner. Individual tiles were stitched together by optimizing the cross-correlation of adjacent tiles and subsequent linear blending. In order to highlight micrometric and submicrometric structure, reduce scattering effects, and filter out spatial features caused by

inhomogeneous illumination, an algorithm based on scale space theory [14] was applied to the individual tiles. The algorithm works by separately applying two Gaussian filters with σ = 35 (yielding F_{35}) and σ = 150 (yielding F_{150}). From the original tile image *I,* the scale-space filtered tile image I_{SSF} is then obtained through:

$$I_{SSF} = I - F_{35} + F_{150} \tag{21.1}$$

This reduces each image to scales $150 < \sqrt{t} < 35$. The scale-space filtered composite images were then intensity stretched and—in case of the 370–410, 412–438, and 499–529 nm emission filters—combined into false color images.

In parallel, numerical analysis of the recorded images was performed to detect statistical differences in luminescence behavior between the different zinc white paint layers. These statistical differences could then be used as evidence for the use of different batches of zinc white throughout the painting, which can help explain the macroscale luminescence of *The Woodcutters* and provide information about its production process.

First, particle sizes—expressed as σ_p—were estimated based on the 2D autocorrelation matrix of $\sqrt{t} < 35$ scale-space filtered images. Then, a set number of particles in each image were integrated within a $2\sigma_p$ radius, of which the median integrated intensity was taken as its metric $M_{L,i}$. Here, the subscripts L and i indicate the paint layer number and emission filter number respectively. To avoid experimental reproducibility issues, ratios were determined from the calculated metrics of each cross-section:

$$R_{L,i,j} = \frac{M_{L,i}}{M_{L,j}} \tag{21.2}$$

Uncertainties in the particle size estimation and the median calculation were combined with the errors resulting from the quantized integration boundaries to yield the overall uncertainty in ratios $R_{L,i,j}$:

$$u_{R_{L,i,j}} = \sqrt{u^2_{p_{L,i,j}} + u^2_{med_{L,i,j}} + u^2_{quant_{L,i,j}}} \tag{21.3}$$

The dissimilarity between two paint layers L and L' is then measured by its combined zeta-score [15]:

$$\zeta_{L,L'} = \frac{\sum_j \left| R_{L,i,j} - R_{L',i,j} \right|}{\sqrt{\sum_j \left(u^2_{R_{L,i,j}} + u^2_{R_{L',i,j}} \right)}} \tag{21.4}$$

Here, the denominator gives the standard deviation of the distribution of the numerator, given that paint layers L and L' have the same chemical composition. The score $\zeta_{L,L'}$ then returns the number of standard deviations that the numerator deviates from its expected value of zero. Purely by chance alone, a score of 1.96 or higher is expected for only 5% of all measurements. When such scores are found, it

is regarded as statistical evidence for the dissimilarity of paint layers L and L', which, in this context, is attributed to the use of different batches of zinc white.

21.3 Results

21.3.1 Instrumental Analysis

Optical Microscopy Optical microscopy images, recorded using visible light and UV illumination, are shown in Fig. 21.2. The three cross-sections show a similar stratigraphy, comprising at least three white paint layers. Layer 3 shows a bright green luminescence under UV illumination, which is predominantly emitted by submicrometric particles. This indicates that the green luminescence on the macroscale—as was hypothesized—indeed originates from the pigment, rather than the binding medium, degradation products, or possible additives. Interestingly, on top of layer 3 in cross-section #3 an additional paint layer appears to be present (layer 4), which does not show the same brightness as layer 3. The inset of Fig. 21.2f shows this layer in detail. In the lower part of each cross-section, a thin translucent layer of glue is visible, which can be seen in cross-section #1 & #3 to be directly applied onto the canvas support.

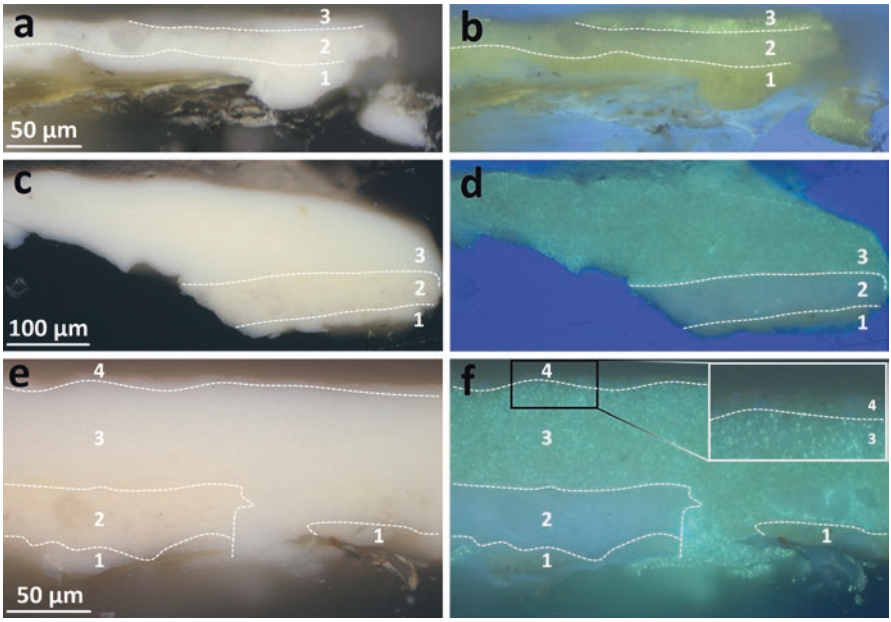

Fig. 21.2 Optical microscopy images of cross-sections #1 (**a, b**, intermediate intensity), #2 (**c, d,** bright intensity), and #3 (**e, f**, low intensity on macroscale). Figures **a, c** & **e** show the images recorded using white light illumination, while figures **b, d** & **f** show the images recorded using UV illumination. The inset in figure f shows a magnification of the region indicated by the black rectangle

Scanning Electron Microscopy SEM backscatter images for the three cross-sections, as well as details of the top layers, are shown in Fig. 21.3a–f. The paint layers that have been discussed in the previous paragraph can be clearly distinguished in each cross-section based on the differences in particle size and electron density. Using EDX analysis (data not shown), layer 1 was determined to contain lead, zinc, and sulfur, layer 2 mostly lead, and layer 3 and 4 only zinc. In an ongoing micro X-ray diffraction study, the lead pigment in layer 1 was identified as lead sulfate (Flemish white), and the lead pigment in layer 2 as lead white. Furthermore, the zinc pigment in layer 1 was identified as zinc white, even though this layer does not show the characteristic green luminescence under UV (Fig. 21.2b, d, and f) that is seen in layers 3 & 4.

On top of each cross-section, a thin unpigmented surface layer was noted (Fig. 21.3b, d, and f). This is especially apparent in cross-sections #1 & #2, which both exhibit a surface layer with an average thickness of 1–2 μm. In cross-section #3, the surface layer has a similar appearance, but was found to be much thinner. The apparent electron density of this thin surface layer is remarkably high, indicating the presence of a substantial inorganic fraction. This presumption was confirmed by EDX analysis, which revealed the presence of mostly zinc, sulfur, and chlorine.

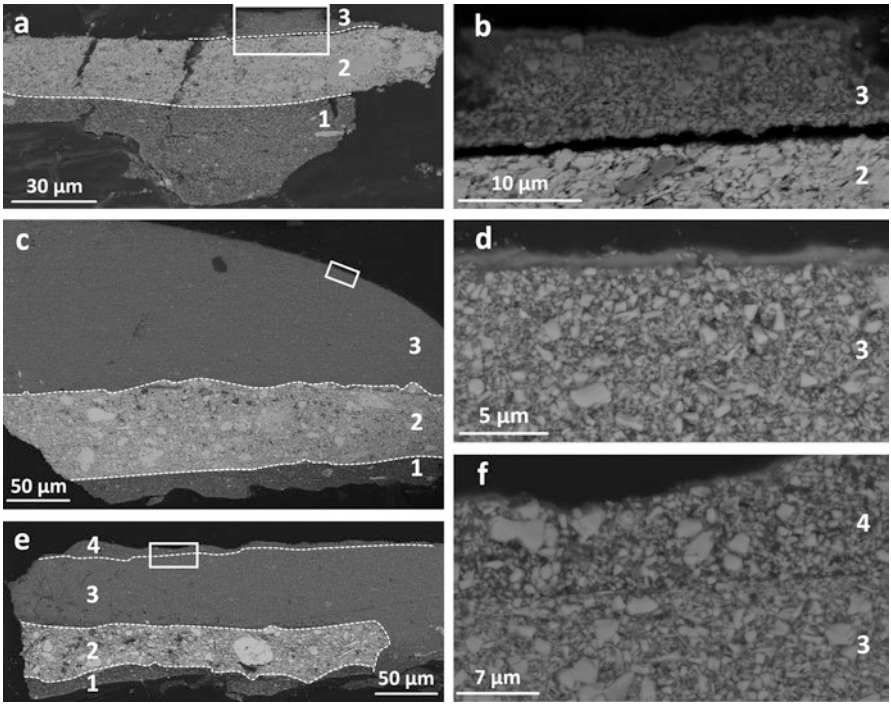

Fig. 21.3 SEM backscatter images of sample #1 (**a, b**, intermediate intensity on macroscale), #2 (**c, d**, bright intensity on macroscale) and #3 (**e, f**, low intensity on macroscale). White rectangles in figures **a, c** & **e** indicate regions of interest of which magnified images are shown in figures **b, d** & **f**

S-DUV-PL Micro-Imaging Figures 21.4a–c show the false color images of the three cross-sections, using the 499–529 nm filter for the red channel, the 412–438 nm filter for the green channel, and the 370–410 nm filter for the blue channel. White rectangles indicate regions of interest which are magnified in Fig. 21.4d and e. In the full-scale false color images, zinc white layers 3 & 4 can be clearly distinguished from the other paint layers, due to the vibrant colors which correspond with the differently luminescing zinc white particles. In each cross-section, layer 3 shows a similar color distribution; particles luminescing predominantly in the blue, green, and red emission channels each present in nearly equal concentrations. However, in layer 4 in cross-section #3 (Fig. 21.4e), particles luminescing in the red channel (499–529 nm) are nearly absent.

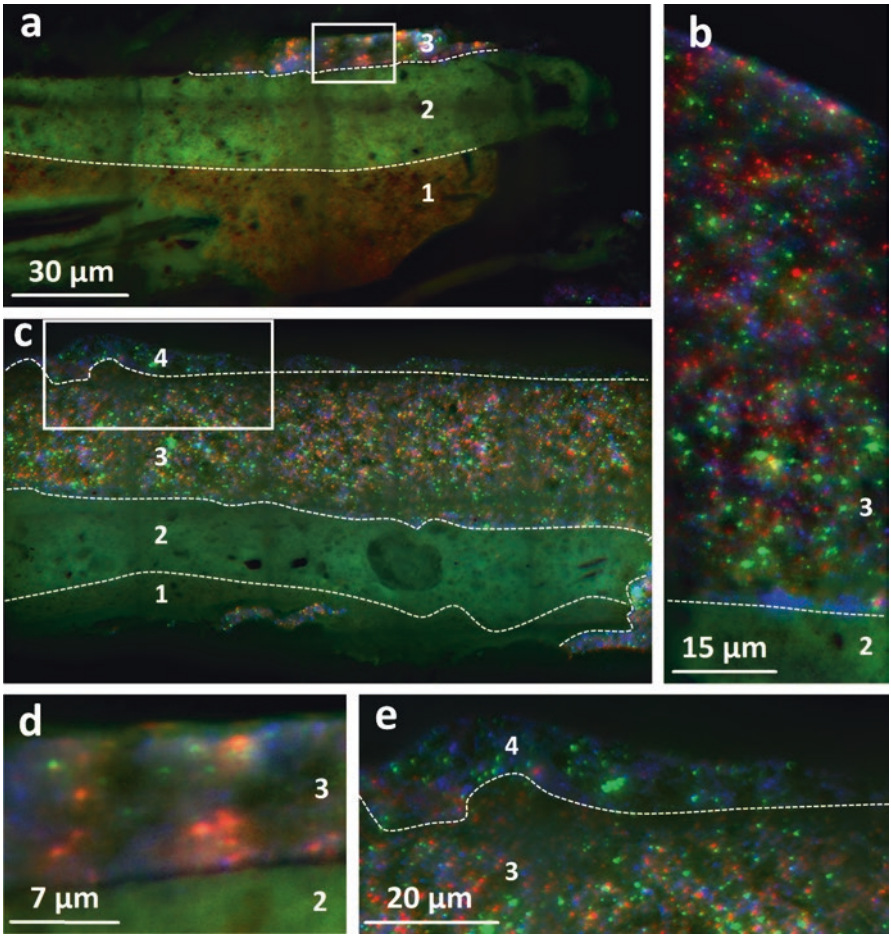

Fig. 21.4 S-DUV-PL false color images of samples #1 (**a, d**), #2 (**b**), and #3 (**c, e**). RGB values were assigned to the following emission filters: red: 499–529 nm, green: 412–438 nm, and blue: 370–410 nm

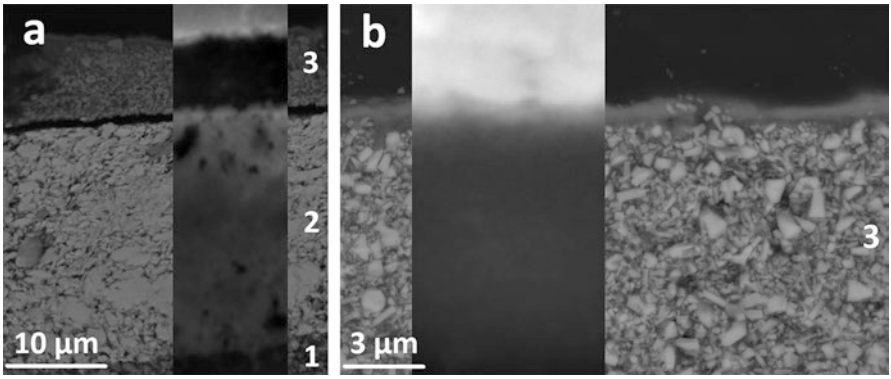

Fig. 21.5 Details of the SEM backscatter images of samples #1 & #2 (Fig. 21.3a and d), superimposed with the photoluminescence images recorded in the 327–353 nm emission range

The presence of zinc white in layer 1 is only evident from some weak luminescence in the 412–438, and 499–529 nm emission ranges. Oddly enough, no signal in the band gap emission range (370–410 nm) could be ascribed to zinc white particles. Although this makes the results obtained from this layer unfit for statistical analysis, this fact alone already shows that this zinc white must come from a different source than the zinc whites used in layers 3 and 4.

Figures 21.5a and b show details of the top of cross-sections #1 & #2, in which thin unpigmented surface layers could be observed in the SEM backscatter images (Fig. 21.3b and d). Here, the backscatter images are overlapped with those obtained using S-DUV-PL micro-imaging through the 327–353 nm emission filter. In both cross-sections, the thin unpigmented surface layer appears to exhibit some luminescence in the UV.

21.3.2 Image Processing & Statistical Analysis

According to the principles outlined in Sect. 2.3, values of $R_{L,i,j}$ and their uncertainties were calculated for all three ZnO emission ranges: 370–410, 412–438, and 499–529 nm. Even though for the interpretation of the macroscale luminescence of *The Woodcutters* only the 412–438 and 499–529 nm emission filters are directly relevant, the 370–410 nm emission is also included, as the resulting multivariate method of analysis has a higher discriminatory power. Due to the previously mentioned lack of signal from layer 1 in the 370–410 nm emission range, statistical analysis was only performed on zinc white layers 3 and 4.

The results are listed in Table 21.1, where the labels $\#1_{L3}$, $\#2_{L3}$, $\#3_{L3}$, and $\#3_{L4}$ are used to distinguish between layer 3 in cross-sections #1, #2, and #3, and layer 4 in cross-section #3 respectively. The zeta-scores and corresponding *p*-values, meant to quantify the differences between each set of *R*-values, are listed in Table 21.2. These values can be interpreted as the probability that two sets of

Table 21.1 Values of $R_{L,\alpha,\beta}$ and $R_{L,\alpha,\gamma}$ calculated for layer 3 in cross-sections #1, #2 and #3 ($\#1_{L3}$, $\#2_{L3}$, $\#3_{L3}$) and layer 3 in cross-section #3 ($\#3_{L4}$)

L	$R_{L,\alpha,\beta}$	u	$R_{L,\alpha,\gamma}$	u
$\#1_{L3}$	3.4	0.7	0.59	0.1
$\#2_{L3}$	2.5	0.2	0.35	0.04
$\#3_{L3}$	2.4	0.3	0.42	0.07
$\#3_{L4}$	3.2	0.5	1.4	0.3

Table 21.2 Zeta-scores and corresponding p-values calculated by comparing the R-values from Table 21.1 according to Eq. 21.4

L vs. L'	$\zeta_{L,L'}$	p
$\#1_{L3}$ vs. $\#2_{L3}$	1.6	0.11
$\#1_{L3}$ vs. $\#3_{L3}$	1.5	0.13
$\#1_{L3}$ vs. $\#3_{L4}$	1.1	0.27
$\#2_{L3}$ vs. $\#3_{L3}$	0.38	0.70
$\#2_{L3}$ vs. $\#3_{L4}$	3.0	0.0025
$\#3_{L3}$ vs. $\#3_{L4}$	2.8	0.0048

R-values—$\{R_{L,\alpha,\beta}, R_{L,\alpha,\gamma}\}$ and $\{R_{L',\alpha,\beta}, R_{L',\alpha,\gamma}\}$—are found given that paint layers L and L' have the same composition.

21.4 Discussion

21.4.1 Explaining Differences in Luminescence on the Macroscale

Instrumental analysis of the three cross-sections obtained from Bart van der Leck's *The Woodcutters* suggests that the layer build-up of the white background is similar throughout the painting, despite the distinctly different luminescence behavior that can be observed in the three sampling regions when the painting is viewed under UV light (Fig. 21.1b). In each of the three cross-sections, a lead sulfate/zinc white layer (1) and a lead white containing layer (2) can be distinguished, of which layer 1 was identified as the ground layer present on the commercially prepared canvas [3]. On top of layer 2, each cross-section shows at least one layer of zinc white. In cross-section #1 (intermediate luminescence on macroscale), this layer is relatively thin (~10 μm), whereas in cross-sections #2 & #3 (bright and low intensity respectively on macroscale), the zinc white-containing layer is much thicker: 150 μm and 100 μm respectively.

From the zeta-scores listed in Table 21.2, conclusions can be drawn on the use of zinc white throughout Bart van der Leck's *The Woodcutters*. First of all, it is evident from the very low value of $\zeta_{\#2_{L3},\#3_{L3}}$ (0.38) that the zinc white particles visible in layer 3 in cross-section #2 and cross-section #3 are very similar. Comparison of

these two layers with the thin zinc white layer in cross-section #1 returns zeta-scores $\zeta_{\#1_{L3},\#2_{L3}}$ and $\zeta_{\#1_{L3},\#3_{L3}}$ of 1.6 and 1.5 respectively. Although the probability of finding these values or higher is relatively small (0.11 and 0.13 respectively), as per convention, this is regarded as insufficient evidence for dissimilarity. Moreover, it must be noted that the number of particles that could be analyzed in cross-section #1 was about an order of magnitude smaller than on cross-section #2 & #3, which makes a statistical comparison challenging to begin with. The remaining set of zeta-scores $\{\zeta_{\#1_{L3},\#3_{L4}}, \zeta_{\#2_{L3},\#3_{L4}}, \zeta_{\#3_{L3},\#3_{L4}}\}$ expresses the statistical significance of the apparent dissimilarities in photoluminescence behavior between layer 4 in cross-section #3, and the other zinc white paint layers analyzed so far. $\zeta_{\#2_{L3},\#3_{L4}}$ and $\zeta_{\#3_{L3},\#3_{L4}}$ were calculated to be 3.0 and 2.8 respectively, indicating significant differences, with probabilities of only 0.0025 and 0.0048 to occur when the same zinc white was used. At 1.1, $\zeta_{\#1_{L3},\#3_{L4}}$ returns a value that indicates no significant dissimilarities. However, as the number of particles that could be analyzed was small for *both* paint layers, this value is not taken into account in the following discussion.

Examining the *R*-values listed in Table 21.1, the statistical dissimilarity between layer 4 in cross-section #3 and layer 3 on cross-sections #2 & #3 seems mostly due to the much higher value of $R_{\#3_{L4},1,3}$, as compared to $R_{\#2_{L3},1,3}$ and $R_{\#3_{L3},1,3}$. This was in turn found to be caused by a significantly weaker signal measured through the 499–529 nm emission filter on layer 4 in cross-section #3 as compared to layer 3 on cross-sections #2 & #3. These results show that the zinc white used in layer 4 in sampling region #3 differs from the zinc white used in layer 3 in sampling regions #2 & #3. It also demonstrates that the significant differences can be ascribed to the weaker luminescence in the green spectral range of the zinc white used in layer 4, which explains the darker appearance of sampling region #3 under UV at the macroscale.

Based on these statistical results and those obtained from the instrumental analyses, it is now possible to formulate a hypothesis as to how the luminescence behavior of *The Woodcutters* on the macroscale is related to the use of pigment throughout the painting and what purpose the corresponding paint layers likely would have served. From the analysis on cross-sections #1 & #2 it could be concluded that the intermediate and bright intensity of green luminescence (Fig. 21.1b) originate from the same zinc white pigment. Differences in luminescence intensity on the macroscale are therefore ascribed to differences in the thickness of the applied paint layer. It can be noted that the intermediate intensity luminescence is most dominantly present in the regions between color planes, whereas the bright intensity luminescence is often present directly around color planes. This suggests that the thicker zinc white layer was applied as a means to modify the composition of the color planes, hereby possibly overpainting the thinner zinc white layer. The absence of a distinct interface within layer 3 in cross-sections #2 & #3 indicates that, if the thicker zinc white layer was indeed applied on top of the thinner zinc white layer, this application was done wet-in-wet.

Just like the bright intensity luminescence, the low intensity luminescence is also found predominantly in the direct vicinity of color planes. This indicates that layer 4 was also applied with the purpose of modifying the composition of the painting. The interface between layer 3 and 4 in cross-section #3—which is clearly visible in the SEM backscatter image shown in Fig. 21.3f—reveals that layer 4 was only applied when layer 3 was already dry. This means that at least several days had passed since the application of layer 3 before these final adjustments to the composition were made.

21.4.2 Assessing Surface Degradation Phenomena

As can be seen in Fig. 21.5a and b, cross-sections #2 & #3 show a thin, unpigmented zinc-rich surface layer that luminesces in the 327–353 nm emission range. Due to the presence of sulfur in this surface layer, its formation is thought to be a result of the reaction of zinc white with atmospheric sulfur compounds, such as sulfur dioxide (SO_2) and/or hydrogen sulfide (H_2S), producing zinc sulfide (ZnS). ZnS, like ZnO is a II-IV semiconductor with a similarly wide band gap of 3.54 eV (351 nm) at room temperature [16]. Therefore, if ZnS crystallites were indeed formed on the paint-air interface, this would explain the luminescence of the surface layer in the 327–353 nm emission range. Yet, when the signal intensities measured on these thin surface layers through the 327–353 nm emission filter are compared to the intensities of the band gap emission of ZnO measured on the same cross-sections, it must be noted that the ZnO band gap emission is over two orders of magnitude stronger than the emission measured on the surface layers. It is thought that this major discrepancy in band gap emission intensity can be attributed to the nanometric size the ZnS crystallites would have, given that they cannot be resolved using SEM at 5000x magnification (Fig. 21.3d). Such nanoparticles, formed in a complex chemical environment, are expected to have severely distorted electronic band structures due to high concentrations of surface states, impurities, and other crystal defects. These severe distortions can make non-radiative relaxation and radiative relaxation through trap-states dominant, thereby reducing the observed band gap emission. If the hypothesis of the formation of ZnS nanoparticles on the painting surface is correct, emission at longer wavelengths is therefore also expected. Such emission can most prominently be seen in the false color image in Fig. 21.4d, where the thin surface layer has a distinct green appearance, indicating emission in the 412–438 nm spectral region. It has been shown previously that ZnS nanoparticles with an average particle size of 1.24 nm exhibit an emission band in this exact spectral region, which is ascribed to the nanoparticles' abundant surface states [17].

The likely degradative origin of the surface layer and its absence in cross-section #3 suggests that there are differences in the chemical properties of these two different varieties of zinc white. Whereas the one used in layer 3 seems very susceptible to reaction with atmospheric sulfur compounds, the variety used in layer 4 appears far less prone to be converted to ZnS. As the only noticeable differences between the two varieties of zinc white show up in their photoluminescence behavior, it is

hypothesized that the reactivity of zinc white and the concentrations of certain crystal defects are related.

21.5 Conclusion

Using a combination of instrumental and statistical analysis, the use and degradation of zinc white in Bart van der Leck's *The Woodcutters* was investigated. The results provide an explanation as to why the white background of the painting has such an inhomogeneous appearance under UV illumination (Fig. 21.1b). It could be concluded that the intermediate intensity luminescence—that appears in the painting for instance in sampling region #1—indicates the presence of a thin zinc white layer that was applied in the background, most likely in an early stage of the painting process. The bright intensity luminescence (e.g. sampling region #2) was found to correspond with a more thickly applied paint layer that contains the same variety of zinc white. These thick layers were applied to modify the composition, possibly by overpainting the previously applied thin zinc white layer wet-in-wet. The low intensity luminescence (e.g. sampling region #3) appears to relate to compositional adjustments that were made by Van der Leck in a later stage using a different variety of zinc white pigment. It is possible that these changes were made several days, weeks, or even months later, after a major part of the composition was already finished. These results demonstrate how—using a multispectral photoluminescence approach—three different varieties of zinc white can be distinguished in a set of historical paint cross-sections.

A thin, unpigmented surface layer was observed in cross-sections #1 and #2. Based on its luminescence in the 327–353 and 412–438 nm spectral regions and its relatively high electron density, it is hypothesized that this surface layer is the result of a reaction between zinc white and atmospheric sulfur compounds, forming nanometric ZnS crystallites. The nearly unaffected appearance of layer 4 in cross-section #3 suggests that significant differences in reactivity exist between differently luminescing varieties of zinc white. Given the well-documented relation between the photoluminescence behavior of zinc white and its crystal defects, it is proposed that a link may exist between defects in the ZnO crystal structure and its reactivity. Further research into this relationship and how it extends to its reactivity towards paint components may help explain why zinc white degradation phenomena vary so widely among paintings. Furthermore, revealing these possible relationships could pave the road for non-invasive risk assessment that is based on the luminescence properties of the paint surface.

Acknowledgments The authors would like to express their gratitude to Matthieu Réfrégiers & Frédéric Jamme (DISCO beamline, SOLEIL synchrotron) for their assistance at the beamline and to Victor Gonzalez for providing the μ-XRD maps used for pigment identification. The authors gratefully acknowledge financial support from The Bennink Foundation and the Access to Research Infrastructures activity in the Horizon 2020 Programme of the EU (IPERION CH Grant Agreement n. 654028).

References

1. Hilhorst C, Wijnia, L (2017) Chronologie. In: De uitvinding van een nieuwe kunst, Piet Mondriaan & Bart van der Leck, Laren 1916–1918, Gemeentemuseum Den Haag/WBooks, Den Haag/Zwolle, p 11–57
2. Janssen H (2017) Inleiding. In: De uitvinding van een nieuwe kunst, Piet Mondriaan & Bart van der Leck, Laren 1916–1918, Gemeentemuseum Den Haag/WBooks, Den Haag/Zwolle, p 7–10
3. Albrecht M, Koenen J (2017) Meer dan het oog ziet: een analyse van drie schilderijen van Bart van der Leck. In: De uitvinding van een nieuwe kunst, Piet Mondriaan & Bart van der Leck, Laren 1916–1918, Gemeentemuseum Den Haag/WBooks, Den Haag/Zwolle, p 147–156
4. De La Rie E R (1982) Fluorescence of Paint and Varnish Layers (Part I). Studies Conserv 27:1–7
5. De La Rie E R (1982) Fluorescence of Paint and Varnish Layers (Part II). Studies Conserv 27:65–69
6. Bertrand L, Réfrégiers M, Berrie B H, Échard J-P, Thoury M (2013) A multiscalar photoluminescence approach to discriminate among semiconducting historical zinc white pigments. Analyst 138:4463–4469
7. De La Rie E R (1982) Fluorescence of Paint and Varnish Layers (Part III). Studies Conserv 27:102–108
8. Broadway M, Sutherland K, Biolcati, V, Casadio, F (2018) Mastery of materials: Sargent's watercolors at the Art Institute of Chicago. In: John Singer Sargent & Chicago's gilded age, Art Institute of Chicago, Chicago, p 188–190
9. Özgür, Ü Alivov, Y I, Liu, C, Teke, A, Reshchikov, M A, Dogan, S, Avrutin, V, Cho S-J, Morkoc, H J (2005) A comprehensive review of ZnO materials and devices. Appl Phys 98:041301
10. Djurisic A B, Leung Y H, Tam K H, Hsu Y F, Ding L, Ge W K, Zhong Y C, Wong K S, Chan W K, Tam H L, Cheah K W, Kwok W M, Phillips D L (2007) Defect emissions in ZnO nanostructures. Nanotechnology 18:095702
11. Giuliani A, Jamme F, Rouam V, Wien F, Giorgetta J-L, Lagarde B, Chubar O, Bac S, Yao I, Rey S, Herbeaux C, Marlats J-L, Zerbib D, Polack F, Réfrégiers M (2009) DISCO: a low-energy multipurpose beamline at synchrotron SOLEIL. J Synchrotron Radiat 16:835–841
12. Thoury M, Echard J-P, Refregiers M, Berrie B H, Nevin A, Jamme F, Bertrand L (2011) Synchrotron UV-Visible multispectral luminescence microimaging of historical samples. Anal Chem 83:1737–1745
13. Hageraats S, Keune K, Réfrégiers M, Van Loon A, Berrie B, Thoury M (2019) Synchrotron Deep-UV Photoluminescence Imaging for the Submicrometer Analysis of Chemically Altered Zinc White Oil Paints. Anal Chem DOI: 10.1021/acs.analchem.9b02443
14. Lindeberg T J (1994) Scale-space theory: A basic tool for analysing structures at different scales Appl Stat 21:225–270
15. Analytical Methods Committee (2016) z-Scores and other scores in chemical proficiency testing-their meanings, and some common misconceptions. Anal Methods 8:5553–5555
16. Yongnian Y, Hickey C F, Gibson U J (1987) ZnS molecular beam epitaxy on silicon substrates. Thin Solid Films 151:207–214
17. Chen W, Wang Z, Lin Z, Lin L (1997) Absorption and luminescence of the surface states in ZnS nanoparticles J Appl Phys 82:3111–3115